



Single-molecule imaging of organic semiconductors: Toward nanoscale insights into photophysics and molecular packing

W.E.B. Shepherd^a, R. Grollman^a, A. Robertson^a, K. Paudel^a, R. Hallani^b, M.A. Loth^b, J.E. Anthony^b, O. Ostroverkhova^{a,*}

^a Department of Physics, Oregon State University, Corvallis, OR 97331, United States

^b Department of Chemistry, University of Kentucky, Lexington, KY 40506, United States

ARTICLE INFO

Article history:

Received 9 January 2015

In final form 11 April 2015

Available online 18 April 2015

ABSTRACT

Photophysical properties of functionalized anthradithiophene (ADT) and pentacene (Pn) derivatives, as well as energy and charge transfer properties of donor–acceptor (D/A) pairs of these derivatives, are presented. The molecules studied were imaged on the single-molecule level in a polymeric and in a functionalized benzothiophene (BTBTB) crystalline host using room-temperature wide-field epifluorescence microscopy. The BTBTB host imposed orientational constraints on the guest molecules, depending on their functionalization. Flexibility of functionalization of both guest (ADT, Pn) and host (BTBTB) molecules can be used for systematic studies of nanoscale morphology and photophysics of D/A organic semiconductor bulk heterojunctions using single-molecule fluorescence microscopy.

© 2015 Elsevier B.V. All rights reserved.

1. Introduction

Organic semiconductors have attracted attention due to their potential applications in a variety of (opto)electronic devices including organic thin-film transistors (TFTs), light-emitting diodes, solar cells, photorefractive (PR) holographic displays, and many others [1]. A large subset of these applications, such as solar cells, photodetectors, and PR devices relies on efficient charge carrier photogeneration. Most successful materials for such applications involve donor–acceptor (D/A) bulk heterojunctions (BHJs), properties of which rely on photoinduced D/A interactions. These include charge transfer (CT) and Förster resonant energy transfer (FRET) that depend both on the photophysical properties of donor and acceptor molecules and on their packing at the D/A interface [2–7]. However, nanoscale morphology of D/A BHJs [8], as well as the effect of local nanoenvironment on the molecular photophysics

of donor and acceptor molecules and on their interactions, are difficult to study systematically, due to inherent inhomogeneity of BHJs and lack of necessary spatial resolution. Therefore, it is important to develop the capability that enables such systematic studies, and to identify suitable model systems that utilize technologically relevant organic semiconductors.

Single-molecule fluorescence spectroscopy (SMFS) has been widely utilized in probing nanoscale interactions and local nanoenvironments in a variety of media including biological systems, polymers, and crystals [9–11]. Single molecules (SMs) have been used as sensitive probes of local changes in polarity, viscosity, relaxation dynamics of the host, and acoustic resonances [12–14] in various heterogeneous environments. SM-level imaging of molecular orientations has provided key nanoscale information on the molecular packing in the solid and on the interfaces [15–19]. Additionally, there has been considerable interest in utilizing SMs as probes of conduction and exciton dynamics in organic semiconductors [20–23]. However, difficulties in finding a suitable model system that meets requirements of SMFS (which include high photostability and high fluorescence quantum yield (QY) of the guest molecules and absence of guest–host interactions, such as intermolecular intersystem crossing, that lead to fluorescence quenching) [24] and provides tunable properties of the molecule and of the environment necessary for systematic studies, limits SMFS studies to only a handful of materials of relevance to organic semiconductor devices [16,20,21,23].

In this letter, we present photophysical properties of functionalized acene and acene-thiophene derivatives (Figure 1) suitable for

Abbreviations: ADT, anthradithiophene; BHJ, bulk heterojunction; BTBTB, benzothiophene; CT, charge transfer; D/A, donor–acceptor; DCDHF, dicyanomethylenedihydrofuran; FRET, Förster resonant energy transfer; HOMO, highest occupied molecular orbital; LUMO, lowest unoccupied molecular orbital; NODIPS, (n-octyldiisopropylsilyl)ethynyl; QY, quantum yield; PMMA, poly(methyl)methacrylate; Pn, pentacene; PR, photorefractive; SM, single molecule; SMFS, single molecule fluorescence spectroscopy; TCHS, (tricyclohexylsilyl)ethynyl; TES, (triethylsilyl)ethynyl; TFT, thin film transistor; TIPS, (triisopropylsilyl)ethynyl; XRD, X-ray diffraction.

* Corresponding author.

E-mail address: oksana@science.oregonstate.edu (O. Ostroverkhova).

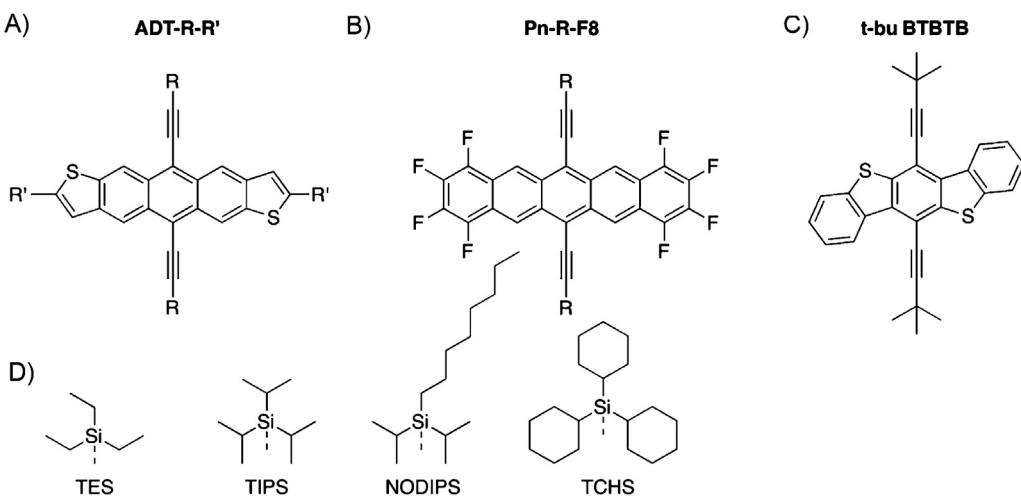


Figure 1. Molecular structures of (a) ADT-R-R', (b) Pn-R-F8, and (c) t-bu BTBTB molecules used in our studies. In (a), R' = F for ADT-TES-F and R' = CN for ADT-TIPS-CN. (d) Structures of the side groups R (R=TES, TIPS, NODIPS, TCHS).

systematic SMFS studies of processes pertinent to nanoscale-level understanding of D/A BHJs: molecular photophysics, molecular packing, and photoinduced intermolecular interactions. These derivatives are of interest due to the following reasons: (1) they are solution-processable organic semiconductors that have been extensively studied in TFTs and solar cells [6,25–27], (2) they can be functionalized to either tune photophysical parameters of the molecule itself or to change the molecular packing in the solid state (e.g. by changing R' and R groups, respectively, Figure 1) [3,5,6], thus enabling systematic studies of effects of substitutions and of local nanoenvironment on the molecular photophysics and packing, and (3) D/A combinations of these molecules exhibit FRET and/or emissive CT state formation (exciplex) [2,5,28,29], which could be utilized in probing nanoscale D/A morphology and effects of local nanoenvironment on photoinduced D/A interactions [8], using SMFS techniques.

2. Experimental

2.1. Materials

Molecules used in our studies as donors and acceptors, and as guests embedded in a solid host for SMFS, are functionalized anthradithiophene (ADT) derivatives with (triethylsilyl)ethynyl (TES) and (triisopropylsilyl)ethynyl (TIPS) side groups (ADT-TES-F and ADT-TIPS-CN, Figure 1a) and pentacene (Pn) derivatives (Figure 1b) with TIPS, NODIPS ((n-octyldiisopropylsilyl)ethynyl), or TCHS ((tricyclohexylsilyl)ethynyl) side groups (Figure 1d). The ADT-TES-F derivative is a high-performance organic semiconductor, solution-deposited films of which exhibit charge carrier mobilities of >1.5 cm²/(Vs) in spin-cast TFTs [25,30], high photoconductive gains, and fast charge carrier photogeneration [3,29,31]. In pristine films of the Pn-TIPS-F8 derivative, ambipolar TFT mobilities of up to 0.33 cm²/(Vs) were obtained [32,33]. Both ADT-TIPS-CN and Pn-R-F8 (R=TIPS, NODIPS, TCHS) derivatives have been utilized as acceptors in D/A BHJs with polymer or ADT-TES-F donors [2,4,5,27–29]. In pristine films, ADT-R-R' and Pn-R-F8 derivatives under study exhibit π-stacking² with R-groups controlling the packing motif [6].

As host matrices, we chose a functionalized benzothiophene (BTBTB) derivative t-bu BTBTB (6,12-bis[2-(t-butyl)ethynyl]benzo[1,2-b:4,5-b']bis(1)benzothiophene) (Figure 1c) and poly(methyl)methacrylate (PMMA) which were previously utilized in our studies of photoconductivity in

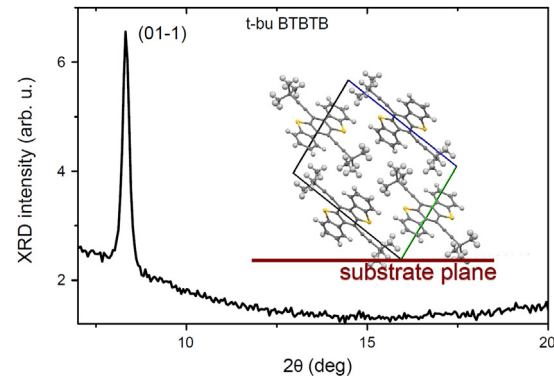


Figure 2. XRD results for out-of-plane structures in spin-cast t-bu BTBTB films. Inset shows alignment of the t-bu BTBTB molecules on the substrate consistent with the (0 1 –1) crystallite orientation as revealed by the XRD.

ADT-TES-F-doped thin-film devices [31]. Both t-bu BTBTB and PMMA hosts have considerably larger HOMO-LUMO gaps (3.52 eV and 5.6 eV, respectively) [31] than ADT and Pn guest molecules (1.9–2.3 eV, depending on the derivative) [5], and no guest-to-host FRET or CT were observed in either guest–host system (Figure S2). The t-bu BTBTB derivative exhibits 1D “slip-stack” π-stacking and crystallizes in a triclinic structure with unit cell parameters $a = 6.3 \text{ \AA}$, $b = 12.6 \text{ \AA}$, $c = 15.9 \text{ \AA}$, $\alpha = 96.1^\circ$, $\beta = 98.5^\circ$, and $\gamma = 102.3^\circ$ (inset of Figure 2). Spin-cast t-bu BTBTB films exhibit crystalline order with a dominant (0 1 –1) crystallite orientation, confirmed by X-ray diffraction (XRD), Figure 2. The lowest-energy absorption/fluorescence maxima in thin t-bu BTBTB films are at 405/415 nm [34], which enables the utility of t-bu BTBTB as a non-emissive host for SM imaging at 532 nm and 633 nm. Functionalized BTBTB derivatives [35] are photoconductive under UV excitation [34], and they have been utilized in solution-deposited field effect transistors exhibiting charge carrier mobilities reaching 1.7 cm²/(Vs) [36], 7 cm²/(Vs) [37], and 31.3 cm²/(Vs) [38], depending on functionalization of the molecule and on device fabrication.

2.2. Sample preparation

For our studies, several types of spin-cast films were prepared: (i) ADT-R-R' or Pn-R-F8 guest molecules at 10^{-10} M concentrations in the PMMA or t-bu BTBTB hosts, for SMFS; (ii) same as (i), but

Table 1

Photophysical properties of ADT-R-R' and Pn-R-F8 molecules in solutions and solid hosts.

| Molecule | $\lambda_{\text{abs}}^{\text{a}}$ (nm) | $\lambda_{\text{em}}^{\text{a}}$ (nm) | $\varepsilon_{\text{max}}^{\text{b}}$ (M ⁻¹ cm ⁻¹) | Φ_F^{c} (PMMA) | τ^{d} (ns) (PMMA) | Φ_B^{e} (10 ⁻⁶) PMMA ^e | $N_{\text{tot}}^{\text{f}}$ (10 ⁵) PMMA ^f | $N_{\text{tot,det}}^{\text{g}}$ (10 ⁵) PMMA ^g (N _{tot,em}) | $N_{\text{tot,det}}^{\text{h}}$ (10 ⁵) t-bu BTBTB ^h |
|--------------|---|--|--|-------------------------------|-------------------------------------|---|--|---|--|
| ADT-TES-F | 525 | 532 | 40,400 | 0.70 (0.90) | 9.4 (12.1) | 1.1 ± 0.2 | 8.2 | 0.35 ± 0.02 (7.7 ± 0.5) | – |
| ADT-TIPS-CN | 579 | 588 | 33,000 | 0.76 (0.89) | 12.7 (14.9) | 2.5 ± 0.5 | 3.6 | 0.29 ± 0.01 (2.4 ± 0.1) | – |
| Pn-TIPS-F8 | 632 | 644 | 22,200 | 0.60 (0.80) | 9.4 (12.5) | 1.9 ± 0.5 | 4.2 | 0.50 ± 0.05 (4.7 ± 0.5) | 0.28 ± 0.03 ⁱ |
| Pn-NODIPS-F8 | 632 | 645 | 29,200 | 0.53 (0.67) | 6.4 (8.1) | 1.2 ± 0.2 | 5.6 | 0.40 ± 0.03 (3.8 ± 0.3) | 0.38 ± 0.03 |
| Pn-TCHS-F8 | 635 | 644 | 19,400 | 0.61 (0.82) | 8.7 (11.7) | 1.0 ± 0.2 | 8.2 | 1.0 ± 0.1 (9.4 ± 0.9) | 0.31 ± 0.01 |

^a Wavelengths of lowest energy absorption maximum or of maximal fluorescence emission (Figure S1), measured in dilute toluene solutions.^b Molar extinction coefficient at the wavelength of maximal absorption λ_{abs} in toluene.^c Fluorescence QY in toluene. The values in parentheses are from “bulk” samples in PMMA.^d Fluorescence lifetime in toluene. The values in parentheses are from “bulk” samples in PMMA.^e Photobleaching QY of Eq. (1) obtained in “bulk” samples in PMMA. Error reflects sample-to-sample variation.^f Total number of emitted photons in PMMA calculated using $N_{\text{tot}} = \Phi_F / \Phi_B$.^g Mean number of total detected photons obtained from single exponential fits to SM histograms (such as that in Figure 4b) in the PMMA host. The value in parentheses is the mean number of total photons emitted by the molecule calculated from the number of total detected photons as $N_{\text{tot,em}} = N_{\text{tot,det}} / \eta_{\text{coll}}$, where η_{coll} is the collection efficiency of Eq. (2).^h Mean number of total detected photons obtained from single exponential fits to SM histograms (such as that in Figure 4b) in the t-bu BTBTB host.ⁱ Based on 29 molecules whose trajectories could be reliably analyzed, as compared to, for example, 169 (102) molecules in the case of Pn-TCHS-F8 (Pn-NODIPS-F8) in t-bu BTBTB (see Section 2). This is due to molecular orientation constraints (discussed in the text) which reduced signal-to-noise ratio in the majority of fluorescence trajectories of Pn-TIPS-F8 molecules in the t-bu BTBTB host.

at higher guest concentrations (“bulk” samples), for fluorescence lifetime, quantum yield (QY), and photobleaching QY measurements; and (iii) 50/50 mixtures of ADT-TES-F and Pn-R-F8 in PMMA for FRET measurements. Dilute solutions of ADT-R-R' and Pn-R-F8 molecules in toluene were also prepared for measurements of several photophysical parameters of Table 1 [3]. Details of sample preparation for each type of the sample can be found in the Supplementary Material.

2.3. Measurements of photophysical parameters and single molecule imaging

Details of measurements of molar absorptivity (ε), fluorescence QY (Φ_F), and fluorescence lifetimes (τ) of Table 1, as well as of the photobleaching time constant τ_B , can be found in the Supplementary Material. All measurements were performed at room temperature in air, unless stated otherwise. The photobleaching QYs (Φ_B) were calculated using [39]

$$\Phi_B = \frac{1}{\tau_B \sigma_\lambda I_\lambda / (hc/\lambda)} \quad (1)$$

where σ_λ is the absorption cross-section at the wavelength of excitation (λ) (see Supplementary Material), I_λ is the excitation intensity, h is the Planck constant, and c is the speed of light. From photobleaching QY Φ_B and fluorescence QY Φ_F , the total number of photons emitted by the molecule was obtained using $N_{\text{tot}} = \Phi_F / \Phi_B$ [39].

Epi-fluorescence imaging of single Pn-R-F8 (ADT-R-R') molecules was performed under circularly polarized 633 nm (532 nm) wide-field illumination using an Olympus IX-71 inverted microscope with a 100× UPlanSApo (NA 1.4) oil objective and an Andor iXon EMCCD (DU-897) detector. The 560DCLP (Omega Optical) and HQ537LP (Chroma Tech.) filter combination was used for imaging at 532 nm. At 633 nm excitation, z633rdc and HQ645LP (both from Chroma Tech.) filters were used. Collection efficiency was determined according to

$$\eta_{\text{coll}} = \eta_Q T_{\text{ang}} T_{\text{opt}} T_{\text{filt}} \quad (2)$$

where η_Q is the quantum efficiency of the camera (85–94%, depending on the fluorescence emission spectrum of the molecule), T_{ang} is the angular collection factor, T_{opt} is the collection factor through the microscope optics (62–68%), and T_{filt} is the transmission through the dichroic and emission filters (21–65%) [39]. For a single dipole

emitter aligned horizontally (i.e. when the polar angle θ between the transition dipole moment of the molecule and the substrate normal is 90°), we estimated T_{ang} to be ~34% using Ha et al. [40], which is similar to 38% used by Lord et al. [39] based on Ref. [41]. With these considerations, the upper bound estimate of our collection efficiency is 4.6% for ADT-TES-F, 12.0% for ADT-TIPS-CN, and 10.6% for Pn-R-F8.

Custom MATLAB scripts were used to locate fluorophores and display their time traces. Each time trace was examined for confirmation of digital blinking or photobleaching. “On” and “off” counts were differentiated using a threshold of three standard deviations of the “off” level noise above the “off” level. The counts were converted to detected photons using the manufacturer-provided analog-to-digital conversion factor and the EMCCD gain. The total detected number of photons was calculated by integrating time traces (with background subtracted) for each fluorophore over the entire lifetime period. Fluorescence trajectories of the following number of molecules were analyzed: 342 (78) for ADT-TIPS-CN (ADT-TES-F) in PMMA, 208 (169) for Pn-TCHS-F8 in PMMA (t-bu BTBTB), 212 (102) for Pn-NODIPS-F8 in PMMA (t-bu BTBTB), and 196 (29) for Pn-TIPS-F8 in PMMA (t-bu BTBTB). A considerably smaller number of analyzable Pn-TIPS-F8 SM traces in t-bu BTBTB was attributed to orientational constraints imposed by the t-bu BTBTB host, as discussed below, which reduced signal-to-noise ratio in this system. Histograms of the number of detected photons (N) were fit to a single-exponential function ($\sim \exp[-N/N_{\text{tot,det}}]$) to determine the mean number of detected photons $N_{\text{tot,det}}$ in Table 1. The number of emitted photons, $N_{\text{tot,em}}$ in Table 1 was calculated by dividing $N_{\text{tot,det}}$ by the collection efficiency η_{coll} of Eq. (2).

Polarization dependence of SM fluorescence was measured in a set up similar to that described above, but a linear polarizer was added to change the polarization of the excitation light in steps of 22.5°. The excitation light was turned off for ~2–5 s as the polarizer rotated to the next setting before the excitation light was turned back on. At each polarizer setting, the data during the time interval at which the molecule was excited were averaged. Traces with blinking events (<3% of all traces analyzed) were excluded from the analysis. Polarization-dependent time traces from 391 (513, 210) molecules of Pn-TCHS-F8 (Pn-NODIPS, Pn-TIPS-F8) in PMMA and 4575 (2991) of Pn-TCHS-F8 (Pn-NODIPS-F8) in t-bu BTBTB were examined. Similar procedure could not be carried out on Pn-TIPS-F8 molecules in t-bu BTBTB due to low signals, which prevented reliable analysis. The angle-dependent numbers of photons detected

Table 2

FRET and emissive CT state properties for various D/A systems.

| D/A system | Volume of R^a Å ³ | R_0^b nm | λ_{CT}^c nm | τ_{CT}^d ns | $I_{CT}(D/A)/I_{CT}(D/ADT\text{-TIPS-CN})^e$ |
|------------------------|-----------------------------------|------------------|------------------------|---------------------|--|
| ADT-TES-F/ADT-TIPS-CN | 278.5 | 4.8 ^d | 669 ^d | 20 ^d | 1 |
| ADT-TES-F/Pn-TIPS-F8 | 278.5 | 4.2 | 723 ^e | 4.5 ^e | 0.21 ± 0.03 |
| ADT-TES-F/Pn-NODIPS-F8 | 402.5 | 4.5 | 723 ^e | 3.4 ^e | 0.064 ± 0.004 |
| ADT-TES-F/Pn-TCHS-F8 | 469.2 | 4.4 | 711 ^e | 2.2 ^g | 0.021 ± 0.001 |

^a Volume of a side group R of acceptor calculated from crystallographic data. From Ref. [5].^b FRET radius calculated as described in the Supplementary Material. FRET in these D/A systems is observed when the donor and acceptor molecules are separated by a neutral spacer such as PMMA.^c Wavelength of maximal fluorescence emission from the D/A charge transfer (CT) state. The emissive CT state is observed in these systems when a neutral spacer is removed.^d From Ref. [28].^e From Ref. [5].^f Lifetime of the fluorescence emission from the CT state obtained in ADT-TES-F/ADT-TIPS-CN (2 wt%) or ADT-TES-F/Pn-R-F8 (2 wt%) films.^g From Ref. [2].^h Intensity of the CT emission in the ADT-TES-F/Pn-R-F8 (2 wt%) films relative to that in ADT-TES-F/ADT-TIPS-CN (2 wt%) films obtained from integrated spectra of CT emission under same excitation conditions. Error reflects sample-to-sample variation. From Ref. [5].

per 100 ms were divided by the collection efficiency of Eq. (2), modified to exclude T_{ang} , to obtain I_{tot} . The I_{tot} data were then fit with a function [40].

$$I_{tot} = A_0 \cos^2(\varphi - \varphi_0) + I_b \quad (3)$$

where φ_0 is the in-plane dipole angle, φ is the excitation polarization angle, and I_b is the background intensity, to determine A_0 and φ_0 . From these, we obtained histograms of A_0 which were then fit with the Gaussian function $\sim \exp[-(A_0 - \langle A_0 \rangle)^2/\sigma^2]$ to extract $\langle A_0 \rangle$ and σ . In order to establish the lowest A_0 value accessible in our experiments, we performed similar polarization-dependent analysis of the background (due to polarization response of the dichroic mirror and birefringence of the host) which yielded values of up to $A_{0,b} = 14$ photons/100 ms for the PMMA and 16 photons/100 ms for the t-bu BTBTB hosts.

3. Results and discussion

3.1. Photophysics and intermolecular interactions: bulk

Photophysical properties of organic semiconductor molecules used in our studies are summarized in Table 1. Optical absorption and fluorescence properties of similar functionalized materials in solution (Figure S1) and in thin films have been previously studied in detail [2–5,28,31]. Briefly, it has been established that variation in core substitutions resulted in an overall shift in the absorption and fluorescence spectra (e.g. a ~54 nm red-shift in absorption of ADT-R-CN as compared to ADT-R-F in toluene, Table 1 and Figure S1). In contrast, side groups R (e.g. R = TIPS, TCHS, and NODIPS in Pn-R-F8, Table 1 and Figure S1) did not considerably affect spectra molecules in solution [3], but they determined π-stacking properties of the molecules in the solid state, which considerably affected (opto)electronic properties of thin films [3].

High fluorescence QYs, Φ_F , for all molecules studied were obtained in toluene (Table 1); they further improved when molecules were immobilized in a solid host, most likely due to reduction in non-radiative relaxation as a result of suppressed rotational and torsional motion of the molecule [42–44], reaching values of ~0.7–0.9 in PMMA that are comparable with many commonly used SM fluorophores [39,43].

The photobleaching QY, Φ_B , which is the probability that a molecule would photobleach upon absorption of a photon, is shown in Table 1. Partial fluorination of the molecular backbone in functionalized ADT [45], Pn, or hexacene [46] derivatives has been realized as an effective means to improve stability of the molecule against oxidation due to substitution of the most reactive site and electronic structure changes induced by electron-negative

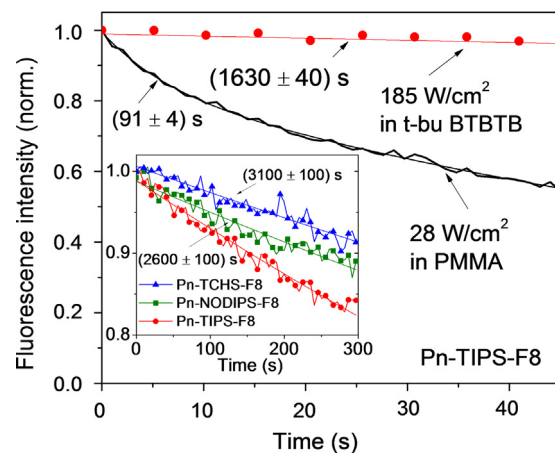


Figure 3. Decay of the fluorescence emission due to photobleaching for Pn-TIPS-F8 in PMMA at 28 W/cm² and in t-bu BTBTB at 185 W/cm² 633 nm illumination. Inset shows data for Pn-TIPS-F8, Pn-NODIPS-F8, and Pn-TCHS-F8 derivatives in t-bu BTBTB at 185 W/cm². Fits with a bi-exponential (in PMMA) and a single-exponential (in t-bu BTBTB) functions and resulting photobleaching times τ_B are also shown.

fluorine substituent [47]. For example, under the same illumination conditions, in air, Pn-R-F8 molecules dispersed in PMMA were considerably more photostable than their counterparts (Pn-R) with no fluorine substitution (Figure S3). The residual photodegradation of ADT-R-R' and Pn-R-F8 derivatives dispersed in PMMA observed in air was significantly reduced in vacuum (Figure S4), which confirms that photobleaching of these molecules is largely due to photoinduced reaction with oxygen [34,48]. In PMMA, the values of Φ_B of $(1\text{--}2.5) \times 10^{-6}$ obtained in ADT and Pn derivatives (Table 1) were comparable with those of commonly used SMFS fluorophores (e.g. dicyanomethylenedihydrofuran (DCDHF) derivatives) in a similar environment [39,43]. Under identical illumination conditions, considerably lower photobleaching decay rates of all derivatives studied were observed in the t-bu BTBTB host, as compared to PMMA (Figure 3) [34]. This could in part be due to reduced oxygen diffusion in the crystalline t-bu BTBTB host as compared to PMMA, a mechanism similar to that behind high photostability of terrylene molecules embedded in a crystalline film of *p*-terphenyl [17]. If one uses Eq. (1), the Φ_B values as low as $(0.6\text{--}1.2) \times 10^{-8}$ are obtained for Pn-R-F8 molecules in t-bu BTBTB. However, as discussed below, the crystalline t-bu BTBTB host imposes constraints on molecular orientations of guest molecules, which prevents accurate determination of Φ_B from Eq. (1) that uses absorption cross-section measured in an isotropic medium with randomly oriented molecules.

The photostability of Pn-R-F8 molecules in both PMMA and t-bu BTBTB hosts depended on the side group R of the guest molecules (Table 1 and Figure 3), so that the Pn-TCHS-F8 molecules (functionalized with large TCHS groups, Table 2) were more photostable than Pn-TIPS-F8 molecules (functionalized with small TIPS groups). This suggests that large side groups R can help reduce access of oxygen to the reactive sites on the molecular backbone, thus lowering the probability of the molecule to undergo oxidative reaction. The values of the total number of emitted photons before the molecule photobleaches (N_{tot} in Table 1) reflect these observations, with more photons emitted by the Pn-TCHS-F8 and Pn-NODIPS-F8 molecules as compared to Pn-TIPS-F8 molecules (e.g. 8.2×10^5 , 5.6×10^5 , and 4.2×10^5 photons, respectively, in PMMA).

Intermolecular interactions between ADT-TES-F donor and ADT-TIPS-CN acceptor molecules have been previously studied in detail [28] and revealed dominance of either FRET or of emissive CT state (exciplex) formation, depending on the D/A distance. In particular, FRET, with a FRET radius R_0 of 4.8 nm was favored when donor and acceptor molecules were separated by PMMA molecules acting as a neutral spacer, whereas the formation of the emissive CT state (Table 2) was the dominant D/A interaction when the PMMA spacer molecules were eliminated (i.e. in ADT-TES-F/ADT-TIPS-CN BHJs) [4,5,28]. Similar trends were observed in the ADT-TES-F/Pn-R-F8 D/A systems: when donor and acceptor molecules were separated by a PMMA spacer, FRET was observed (Figure S5), but when the spacer was eliminated, emissive CT state formation [2,5] was the dominant D/A interaction. Parameters characterizing FRET and the CT state formed between the ADT-TES-F (donor) molecules and ADT-TIPS-CN or Pn-R-F8 (acceptor) molecules are summarized in Table 2. The FRET radius R_0 (calculated assuming that the ADT-TES-F donor and Pn-R-F8 acceptor molecules are immobilized in PMMA, see Supplementary Material) yielded 4.2–4.5 nm (Table 2). The CT state emission considerably depended on the acceptor's R-groups, correlating with the size of R-groups (Table 2). In particular, the CT state was less emissive in a D/A pair with a larger D/A separation, enabled by larger side-groups R on the acceptor molecule [5].

3.2. Photophysics: single molecule level

The ADT-R-R' (Pn-R-F8) molecules of Figure 1 were imaged on the single-molecule level in PMMA and t-bu BTBTB hosts under a 532 nm (633 nm) wide-field excitation. Figure 4a and Figure S6 show examples of fluorescence time trajectories collected from individual molecules of Pn-R-F8 in the PMMA and t-bu BTBTB hosts under wide-field illumination (inset of Figure 4b). In both hosts, up to ~80% molecules did not exhibit blinking (Figure 4a, top and middle), and most blinking molecules experienced only one blinking event (Figure 4a, bottom) before photobleaching. The total number of detected photons for each molecule was determined by integrating SM time traces such as those in Figure 4a to construct histograms. The example histogram, from which the mean number of detected photons per molecule, $N_{\text{tot},\text{det}}$, was obtained using a single exponential fit (see Section 2), is shown in Figure 4b. Because only a fraction of photons emitted by the molecule was detected, the $N_{\text{tot},\text{det}}$ values were considerably lower than N_{tot} calculated from Φ_B (Table 1). However, in PMMA the number of photons emitted by a SM ($N_{\text{tot},\text{em}}$ shown in Table 1 in parentheses), estimated using $N_{\text{tot},\text{det}}$ and the collection efficiency of Eq. (2), yielded values similar to N_{tot} . For example, the SM value $N_{\text{tot},\text{em}}$ of $(7.7 \pm 0.5) \times 10^5$ obtained for ADT-TES-F in PMMA was comparable with a 8.2×10^5 value of the N_{tot} calculated from Φ_B in corresponding "bulk" samples. As with the "bulk" N_{tot} values, the Pn-TCHS-F8 derivative exhibited the highest SM values $N_{\text{tot},\text{em}}$ of the three Pn-R-F8 derivatives in PMMA, reaching $(9.4 \pm 0.9) \times 10^5$ photons. These approach the values of $(1.2\text{--}2.4) \times 10^6$ emitted photons per molecule obtained in demonstrably good SMFS fluorophores such

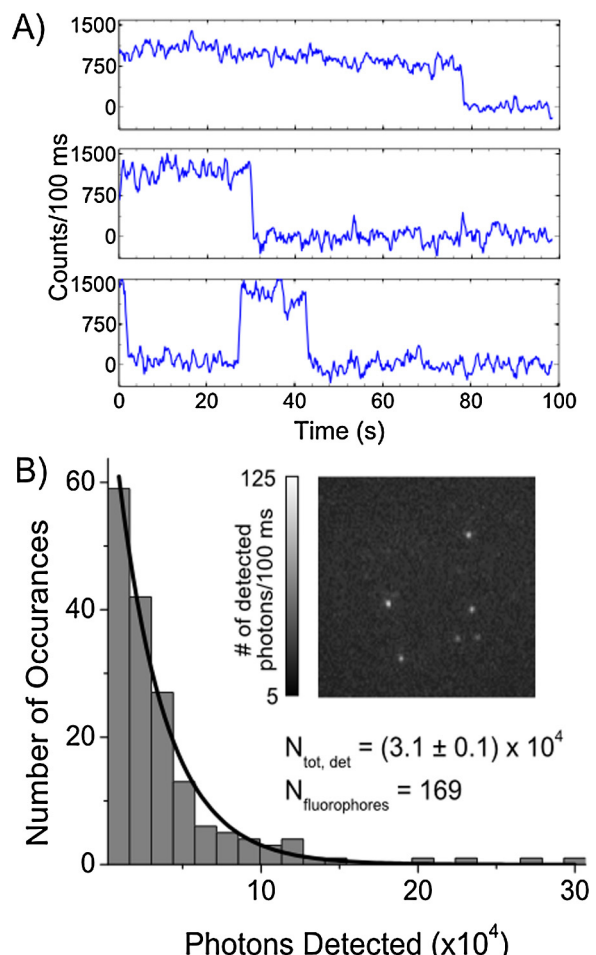


Figure 4. (a) SM fluorescence time trajectories obtained under a wide-field 633 nm excitation at 55 W/cm^2 of Pn-TCHS-F8 in t-bu BTBTB (top) and Pn-TCHS-F8 in PMMA (middle, bottom). (b) Histogram of the total number of detected photons of Pn-TCHS-F8 in t-bu BTBTB from 169 fluorophores. Single-exponential fit and the resulting value of $N_{\text{tot},\text{det}}$ are also included. Inset shows a wide-field epi-fluorescence image of Pn-NODIPS-F8 molecules in the t-bu BTBTB host taken under the conditions listed above.

as DCDHF derivatives or rhodamine 6G under similar conditions [39,43].

Interestingly, in the t-bu BTBTB host the SM $N_{\text{tot},\text{det}}$ values were similar or slightly lower than those in PMMA (Table 1), in spite of considerably higher photostability exhibited by "bulk" samples of Pn-R-F8 in t-bu BTBTB as compared to those in PMMA (Figure 3). This scenario could be realized if the guest molecules resisted photobleaching longer in t-bu BTBTB as compared to PMMA but were constrained by the crystalline t-bu BTBTB host to align with their transition dipole moments nearly parallel to the substrate normal (i.e. resulting in small angles θ in Figure 5d) which is the direction of optical axis in our experiments [17]. In this case, the measured $N_{\text{tot},\text{det}}$ would be considerably lower due to inefficient excitation and reduced detection of the SM emission in our experimental geometry.

To confirm orientational constraints in samples with the t-bu BTBTB host, we studied dependence of the SM emission on the polarization of excitation in both hosts. An example of data is shown in Figure 5a. Modulation in fluorescence emission intensity (I) due to varying angle between the absorption dipole moment (μ) and the electric field (E) of the incoming light ($I \sim |\mu \cdot E|^2$) was observed (Figure 5a), as expected from a single-dipole emitter. Here μ is the transition dipole moment for the $S_0\text{--}S_1$ transition, which in our molecules is aligned with the short axis of the

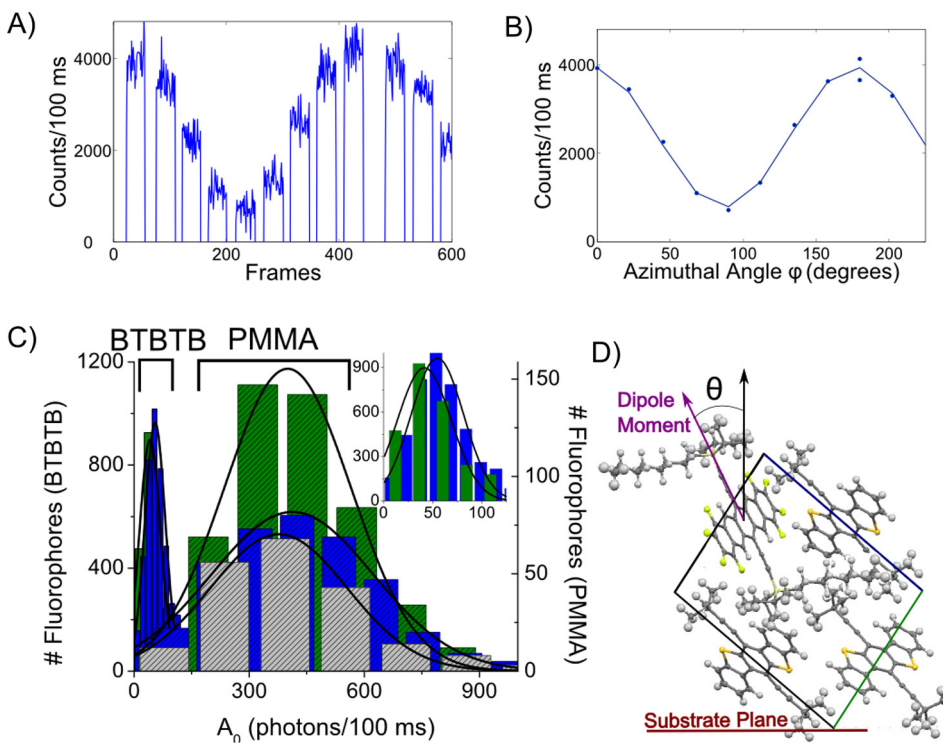


Figure 5. (a) Raw time trace from a Pn-TIPS-F8 fluorophore in PMMA under a 633 nm 28 W/cm² excitation with varying polarization. Time intervals with no data indicate where the light is shuttered as the polarizer rotated to the next setting. For most traces the modulation depth $(I_{\max} - I_{\min})/(I_{\max} - I_b)$ was close to 100%, as further illustrated in Figure S7. (b) Averaged data from the raw time trace with a fit to Eq. (3). (c) Histograms of modulation amplitudes A_0 from fits of the polarization-dependent SM emission data to Eq. (3) (blue: Pn-TCHS-F8, green: Pn-NODIPS-F8, gray: Pn-TIPS-F8). Gaussian fits to the histograms are also shown. The inset shows an expanded view of the histograms obtained for Pn-TCHS-F8 and Pn-NODIPS-F8 in the t-bu BTBTB host. (d) Schematic of a Pn-R-F8 molecule packing in the crystalline t-bu BTBTB host inferred from the SM data (here R=NODIPS). (For interpretation of the references to color in this figure legend, the reader is referred to the web version of this article.)

molecular backbone (Figure 5d) [49]. Most molecules exhibited close to 100% modulation depth so that the modulation amplitude A_0 of Eq. (3) is $I_{\max} - I_{\min}$ with $I_{\min} \approx I_b$ (Figure S7) (here I_{\max} (I_{\min}) is the highest (lowest) emission intensity and I_b is the background intensity attained when the molecule photobleaches). Neither fluorescence trajectory showed evidence of rotational jumps [40]. Following the formalism developed in [40] for a similar experimental geometry, the data were fit with Eq. (3) (Figure 5b), and the phase and amplitude parameters φ_0 and A_0 were determined. No preferential azimuthal orientation φ_0 was observed in either host. Figure 5c shows distributions of A_0 values obtained for Pn-R-F8 molecules in PMMA and t-bu BTBTB hosts, along with Gaussian fits (see Section 2) which were used to obtain the mean values of A_0 ($\langle A_0 \rangle$) and standard deviations (σ) of the distributions. These yielded $\langle A_0 \rangle_{\text{PMMA}} (\sigma_{\text{PMMA}}) = 410 \pm 10$ (299 ± 3), 401 ± 2 (234 ± 5), and 377 ± 4 (250 ± 10) photons/100 ms for Pn-TCHS-F8, Pn-NODIPS-F8, and Pn-TIPS-F8 in PMMA and $\langle A_0 \rangle_{\text{BTBTB}} (\sigma_{\text{BTBTB}}) = 55 \pm 1$ (38 ± 1) and 42 ± 9 (40 ± 20) photons/100 ms for Pn-TCHS-F8 and Pn-NODIPS-F8, respectively, in t-bu BTBTB. Similar (within <9%) $\langle A_0 \rangle_{\text{PMMA}}$ values obtained for all three Pn-R-F8 derivatives are consistent with similar products of molar extinction coefficients and fluorescence QYs of these molecules (Table 1) and the absence of orientational constraints in PMMA. The distribution widths σ_{PMMA} reflect a spread in the polar angle θ (Figure 5d) and in the inhomogeneity of local nanoenvironment experienced by a Pn-R-F8 molecule in PMMA. The largest σ_{PMMA} in the case of Pn-TCHS-F8 as compared to other Pn-R-F8 derivatives may indicate the largest degree of inhomogeneity experienced by Pn-TCHS-F8 molecules, as similar spreads in θ would be expected for all Pn-R-F8 derivatives in PMMA. Considerably smaller values of $\langle A_0 \rangle$ and σ for Pn-R-F8 molecules were observed in the t-bu BTBTB host as compared to PMMA,

which we then sought to relate to constraints in the orientations of the Pn-R-F8 molecules imposed by the t-bu BTBTB host.

The modulation amplitude A_0 of Eq. (3) depends on the polar angle θ between the transition dipole moment of the molecule and the substrate normal ($A_0 \sim \sin^2 \theta$) [50]. It also incorporates a correction due to the polarization mixing in the high-NA objective used in detection of the SM emission [40], so that $A_0 \sim \sin^2 \theta ((K_1 + K_2) \sin^2 \theta + 2K_3 \cos^2 \theta)$, where K_1 , K_2 , and K_3 are parameters which for our objective are equal to 0.332, 0.0065, and 0.106, respectively. (If $\theta=90^\circ$, such correction yields 0.34, which was used to estimate T_{ang} in Eq. (2).) Since no evidence of guest-host interactions that would quench guest fluorescence [24] in the t-bu BTBTB host was observed (see Supplementary Material), we attribute considerably lower values of $\langle A_0 \rangle_{\text{BTBTB}}$ and σ_{BTBTB} , as compared to $\langle A_0 \rangle_{\text{PMMA}}$ and σ_{PMMA} (Figure 5c), to Pn-R-F8 molecule orientations constrained by the t-bu BTBTB host to small polar angles θ (Figure 5d) [17]. Assuming isotropic orientation of Pn-R-F8 molecules in PMMA and an alignment constrained to a narrow range of angles around θ_0 in the t-bu BTBTB host, we estimated an upper bound for the angle θ_0 for the Pn-R-F8 molecules in t-bu BTBTB using the $\langle A_0 \rangle_{\text{PMMA}}/\langle A_0 \rangle_{\text{BTBTB}}$ ratios as described in the Supplementary Material. These estimates yielded $\theta_0 = 20^\circ \pm 1^\circ$ and $18^\circ \pm 2^\circ$ for Pn-TCHS-F8 and Pn-NODIPS-F8, respectively. Since $\langle A_0 \rangle_{\text{BTBTB}}$ for Pn-TIPS-F8 molecules was at or below the highest level of the background variation with the incident polarization $A_{0,b}$, similar analysis using $\langle A_0 \rangle_{\text{BTBTB}} = A_{0,b}$ revealed an upper bound of $\theta_0 \approx 12^\circ$ for Pn-TIPS-F8 in the t-bu BTBTB host. A considerably lower angle θ_0 estimated for Pn-TIPS-F8 as compared to Pn-NODIPS-F8 and Pn-TCHS-F8 in the t-bu BTBTB host may suggest that given a larger free volume (e.g. due to a small TIPS group, as compared to large NODIPS or TCHS groups, Table 2) the Pn-R-F8 molecule

constrained by the crystalline t-bu BTBTB host prefers orientation such that its transition dipole moment is nearly parallel to the substrate normal. Since the BTBTB host can be functionalized to achieve different packing motifs, systematic studies of the host's constraints on the packing of the guest molecules are possible and may improve understanding of formation and properties of organic semiconductor BHJs.

4. Conclusions

In summary, we characterized photophysical properties of functionalized organic semiconductor molecules that enable systematic studies of local environment and molecular packing at nanoscales using SMFS. All derivatives studied were imaged on the single-molecule level in crystalline organic semiconductor (t-bu BTBTB) and polymeric (PMMA) hosts using wide-field illumination at room temperature. The molecules with larger side groups (e.g. Pn-TCHS-F8) were more photostable than those with smaller side groups (e.g. Pn-TIPS-F8) in both hosts studied; several derivatives in PMMA emitted a total number of photons approaching that of standard SMFS fluorophores under similar conditions. The crystalline t-bu BTBTB host imposed orientational constraints on the guest Pn-R-F8 molecule alignment, depending on the guest's side group R. Flexibility of functionalization of guest molecules (ADT-R-R' or Pn-R-F8) and host molecules (t-bu BTBTB) with various side groups R that directly impact molecular packing can be utilized for systematic nanoscale studies of formation and photophysics of organic semiconductor bulk heterojunctions. Photoinduced interactions such as FRET and emissive CT state formation observed in D/A pairs of functionalized ADT-R-R' and Pn-R-F8 derivatives could serve as additional nanoscale probes of intermolecular arrangements at D/A interfaces.

Acknowledgements

We thank Prof. K. A. Willets for helpful discussions, G. Banton for assistance with software development for analysis of single molecule trajectories, Prof. R. J. Twieg for DCDHF, and K. McLelland and Prof. M. Graham for assistance with measurements of fluorescence spectra from D/A samples. This work was supported by the National Science Foundation via CAREER program (DMR-0748671) and DMR-1207309, as well as the SOLAR program (DMR-1035257).

Appendix A. Supplementary data

Supplementary data associated with this article can be found, in the online version, at doi:10.1016/j.cplett.2015.04.014

References

- [1] O. Ostroverkhova, Handbook of organic materials for optical and (photo)electronic devices, Woodhead Publishing, Oxford, 2013.
- [2] K. Paudel, B. Johnson, A. Neunzert, M. Thieme, B. Purushothaman, M.M. Payne, J.E. Anthony, O. Ostroverkhova, *J. Phys. Chem. C* 117 (2013) 24752.
- [3] A.D. Platt, J. Day, S. Subramanian, J.E. Anthony, O. Ostroverkhova, *J. Phys. Chem. C* 113 (2009) 14006.
- [4] A.D. Platt, M.J. Kendrick, M.A. Loth, J.E. Anthony, O. Ostroverkhova, *Phys. Rev. B* 84 (2011) 235209.
- [5] M.J. Kendrick, A. Neunzert, M.M. Payne, B. Purushothaman, B.D. Rose, J.E. Anthony, M.M. Haley, O. Ostroverkhova, *J. Phys. Chem. C* 116 (2012) 18108.
- [6] J.E. Anthony, *Chem. Rev.* 106 (2006) 5028.
- [7] T. Ameri, P. Khoram, J. Min, C.J. Brabec, *Adv. Mater.* 25 (2013) 4245.
- [8] R. Giridharagopal, D.S. Ginger, *J. Phys. Chem. Lett.* 1 (2010) 1160.
- [9] W.E. Moerner, *J. Phys. Chem. B* 106 (2002) 910.
- [10] W.E. Moerner, *Proc. Natl. Acad. Sci. U.S.A.* 104 (2007) 12596.
- [11] W.E. Moerner, M. Orrit, *Science* 283 (1999) 1670.
- [12] K. Wustholz, D. Sluss, B. Kahr, P.J. Reid, *Int. Rev. Phys. Chem.* 27 (2008) 167.
- [13] K.A. Willets, P.R. Callis, W.E. Moerner, *J. Phys. Chem. B* 108 (2004) 10465.
- [14] M.A. Kol'chenko, A.A.L. Nicolet, M.D. Galouzis, C. Hofmann, B. Kozankiewicz, M. Orrit, N. J. Phys. 11 (2009) 023037.
- [15] W. Schroyers, R. Vallee, D. Patra, J. Hofkens, S. Habuchi, T. Vosch, M. Cotlet, K. Mullen, J. Enderlein, F. De Schryver, *J. Am. Chem. Soc.* 126 (2004) 14310.
- [16] A. Thiessen, J. Vogelsang, T. Adachi, F. Steiner, D.A. Vanden Bout, J.M. Lupton, *Proc. Natl. Acad. Sci. U.S.A.* 110 (2013) E3550.
- [17] R. Pfab, J. Zimmerman, C. Hettich, I. Gerhardt, A. Renn, V. Sandoghdar, *Chem. Phys. Lett.* 387 (2004) 490.
- [18] A.P. Bartko, K. Xu, R.M. Dickson, *Phys. Rev. Lett.* 89 (2002) 026101.
- [19] R. Borner, D. Kowanko, S. Krause, C. Von Borczyskowski, C.G. Hubner, *J. Chem. Phys.* 137 (2012) 164202.
- [20] J.M. Lupton, *Adv. Mater.* 22 (2010) 1689.
- [21] B. Kozankiewicz, M. Orrit, *Chem. Soc. Rev.* 43 (2014) 1029.
- [22] J. Bolinger, K.J. Lee, R. Palacios, P.F. Barbara, *J. Phys. Chem. C* 112 (2008) 18608.
- [23] P.F. Barbara, A.J. Gesquiere, S.J. Park, Y.J. Lee, *Acc. Chem. Res.* 38 (2005) 602.
- [24] A.A.L. Nicolet, M.A. Kol'chenko, B. Kozankiewicz, M. Orrit, *J. Chem. Phys.* 124 (2006) 164711.
- [25] D.J. Gundlach, J.E. Royer, S.K. Park, S. Subramanian, O.D. Jurchescu, B.H. Hamadani, A.J. Moad, R.J. Kline, L.C. Teague, O. Kirillov, C.A. Richter, J.G. Kushner, L.J. Richter, S.R. Parkin, T.N. Jackson, J.E. Anthony, *Nat. Mater.* 7 (2008) 216.
- [26] J.E. Anthony, *Chem. Mater.* 23 (2011) 583.
- [27] K.R. Rajesh, K. Paudel, B. Johnson, R. Hallani, J.E. Anthony, O. Ostroverkhova, *J. Photon Energy* 5 (2015) 057208.
- [28] W.E.B. Shepherd, A.D. Platt, M.J. Kendrick, M.A. Loth, J.E. Anthony, O. Ostroverkhova, *J. Phys. Chem. Lett.* 2 (2011) 362.
- [29] K. Paudel, B. Johnson, M. Thieme, M.M. Haley, M.M. Payne, J.E. Anthony, O. Ostroverkhova, *Appl. Phys. Lett.* 105 (2014) 043301.
- [30] S.K. Park, D.A. Mourey, S. Subramanian, J.E. Anthony, T.N. Jackson, *Appl. Phys. Lett.* 93 (2008) 043301.
- [31] W.E.B. Shepherd, A.D. Platt, D. Hofer, O. Ostroverkhova, M.A. Loth, J.E. Anthony, *Appl. Phys. Lett.* 97 (2010) 163303.
- [32] M.L. Tang, A.D. Reichardt, P. Wei, Z. Bao, *J. Am. Chem. Soc.* 131 (2009) 5264.
- [33] C.R. Swartz, S.R. Parkin, J.E. Bullock, J.E. Anthony, A.C. Mayer, G.G. Malliaras, *Org. Lett.* 7 (2005) 3163.
- [34] W.E.B. Shepherd, A.D. Platt, G. Banton, M.A. Loth, J.E. Anthony, O. Ostroverkhova, *Proc. SPIE* 7599 (2010) 75990R.
- [35] K. Takimiya, S. Shinamura, I. Osaka, E. Miyazaki, *Adv. Mater.* 23 (2011) 4347.
- [36] P. Gao, D. Beckmann, H.N. Tsao, X. Feng, V. Enkelmann, M. Baumgarten, W. Pisula, K. Mullen, *Adv. Mater.* 21 (2009) 213.
- [37] A.Y. Amin, K. Reuter, T. Meyer-Friedrichsen, M. Halik, *Langmuir* 27 (2011) 15340.
- [38] H. Minemawari, T. Yamada, H. Matsui, J. Tsutsumi, S. Haas, R. Chiba, R. Kumai, T. Hasegawa, *Nature* 475 (2011) 364.
- [39] S.J. Lord, Z. Lu, H. Wang, K.A. Willets, P.J. Schuck, H.D. Lee, S.Y. Nishimura, R.J. Twieg, W.E. Moerner, *J. Phys. Chem. A* 111 (2007) 8934.
- [40] T.J. Ha, T. Laurence, D.S. Chemla, S. Weiss, *J. Phys. Chem. B* 103 (1999) 6839.
- [41] J. Enderlein, *Opt. Lett.* 25 (2000) 634.
- [42] M.A. Menese-Nava, O. Barbosa-Garcia, L.A. Diaz-Torres, S. Chavez-Cerda, M. Torres-Cisneros, T.A. King, *Opt. Mater.* 17 (2001) 415.
- [43] K.A. Willets, O. Ostroverkhova, M. He, R.J. Twieg, W.E. Moerner, *J. Am. Chem. Soc.* 125 (2003) 1174.
- [44] P. Hrdlořík, J. Krajcovic, D. Vegh, *J. Photochem. Photobiol. A* 144 (2001) 73.
- [45] S. Subramanian, S.K. Park, S.R. Parkin, V. Podzorov, T.N. Jackson, J.E. Anthony, *J. Am. Chem. Soc.* 130 (2008) 2706.
- [46] B. Purushothaman, S.R. Parkin, M.J. Kendrick, D. David, J.W. Ward, L. Yu, N. Stigelin, O.D. Jurchescu, O. Ostroverkhova, J.E. Anthony, *Chem. Commun.* 48 (2012) 8261.
- [47] B. Medina, D. Beljonne, H.J. Egelhaaf, J. Gierschner, *J. Chem. Phys.* 126 (2007) 111101.
- [48] J. Schuster, F. Cichos, C. Von Borczyskowski, *Opt. Spect.* 98 (2005) 712.
- [49] B. Valeur, Molecular Fluorescence: Principles and Applications, Wiley-VCH, Weinheim, 2002.
- [50] J.T. Fourkas, *Opt. Lett.* 26 (2001) 211.